Materials Horizons

Generative machine learning algorithm for lattice structures with superior mechanical properties

Journal:	*Materials Horizons*
Manuscript ID	MH-COM-11-2021-001792.R1
Article Type:	Communication
Date Submitted by the Author:	13-Jan-2022
Complete List of Authors:	Lee, Sangryun; University of California Berkeley, Mechanical Engineering Zhang, Zhizhou ; University of California Berkeley, Mechanical Engineering Gu, Grace; University of California Berkeley, Mechanical Engineering

Generative machine learning algorithm for lattice structures with superior mechanical properties

Sangryun Lee[1], Zhizhou Zhang[1], and Grace X. Gu[1,*]

[1]Department of Mechanical Engineering, University of California, Berkeley, CA 94720, USA

[*]Corresponding author: ggu@berkeley.edu

New concepts

In this work, we propose a novel hybrid neural network and genetic optimization (NN-GO) adaptive method to expand the design space of lattice structures with the aim of further improving their mechanical properties. A key element of our NN-GO method is the utilization of Bézier curves to systematically generate designs where the beam element profile is taken as a design variable. The combination of neural networks for fast inference and genetic optimization for design generation leads to the creation of never-before-seen lattice structures that can be tailored to desired properties. The duality of the proposed method also allows for a feedback loop whereby designs generated by the genetic optimization can be used as new training samples to the neural network, where a new batch of optimized designs can be generated. Moreover, additive manufacturing and compression experiments are conducted to validate the proposed method. This adaptive framework is envisioned to be applicable for the design of lightweight materials with desired properties.

Generative machine learning algorithm for lattice structures with superior mechanical properties

Sangryun Lee[1], Zhizhou Zhang[1], and Grace X. Gu[1,*]

[1]Department of Mechanical Engineering, University of California, Berkeley, CA 94720, USA

[*]Corresponding author: ggu@berkeley.edu

Abstract

Lattice structures are typically made up of a crisscross pattern of beam elements, allowing engineers to distribute material in a more structurally effective way. However, a main challenge in the design of lattice structures is a trade-off between the density and mechanical properties. Current studies have often assumed the cross-sectional area of the beam elements to be uniform for reducing the design complexity. This simplified approach limits the possibility of finding superior designs with optimized weight-to-performance ratios. Here, the optimized shape of the beam elements is investigated using a deep-learning approach with high-order Bézier curves to explore the augmented design space. This is then combined with a hybrid neural network and genetic optimization (NN-GO) adaptive method for the generation of superior lattice structures. In our optimized design, the distribution of material is smartly shifted more towards the joint region, the weakest location of lattice structures, to achieve the highest modulus and strength. This design strikes to balance between two modes of deformation: axial and bending. Thus, the optimized design is efficient for load bearing and energy absorption. To validate our simulations, the optimized design is then fabricated by additive manufacturing and its mechanical properties are evaluated through compression testing. A good correlation between experiments and simulations is observed and the optimized design has outperformed benchmark ones in terms of modulus and strength. We show that the extra design flexibility from high-order Bézier curves allows for a smoother transition between the beam elements which reduces the overall stress concentration profile.

Introduction

Designing lightweight and strong materials has been a long-sought goal in mechanical and materials engineering for decades. Many previous works have tried to develop new materials by introducing physical or chemical bonds between two different materials such as composites and alloys, or tuning microstructures of single materials.[1-6] The lattice structure, especially, inspired by the unit cell of crystalline materials in nature, is one of the most lightweight structures compared to conventional engineering materials.[7, 8] With the recent development of precise additive manufacturing processes, much work has been devoted to understanding the relationship between microstructure and mechanical properties.[9-15] Specifically, microstructures typically need to be tuned depending on the type of the lattice being optimized, such as octet, body-centered, face-centered, diamond or other complicated structures.

One of the inherent limitations of the lattice structure is the reduction of its mechanical properties compared to its base material due to high void fraction.[16] If the lattice structure is viewed as a composite with base material and void phases, the theoretical limit of the modulus (E_{th}) is calculated by using the Voigt limit,[17] expressed as $E_{\text{th}} = \bar{\rho}E_0$ where E_0 is the modulus of the base material and $\bar{\rho}$ is the relative density of the lattice structure. Since the lattice structure typically has at least cubic symmetry, it is difficult to achieve the upper bound of the modulus where the architecture is highly anisotropic. In order to improve mechanical properties at a fixed density, many previous works have designed stiff lattice architectures inspired by various lattice structures seen in nature.[18-20] However, despite intensive research activities, the shape of the beam element in the lattice structure is not typically considered as a design variable to further improve the mechanical properties. The

challenge in exploring variable cross-sections of beam elements arises from the expanded design space that is orders of magnitude larger all while having to formulate relative density constraints for unbiased comparisons.

Consequently, simple geometries parameterized by a few variables have been developed for modeling the beam element. For example, studies have suggested a tapered beam or graded beam element described by two design variables for body-centered (BC) lattice structures.[21, 22] In these works, the BC lattice structure with a modified beam element has a noticeable improvement in elastic stiffness and strength compared to a cylindrical element case. However, a small number of geometric parameters have been used for modeling because it is difficult to work with a large number of design variables when it comes to design and optimization methods. Recently, machine learning algorithms have shown exceptional performance in learning complicated relationships between high-dimensional inputs and outputs. Specifically, by leveraging the fast prediction of neural networks (NNs), previous works designing the optimized microstructure or shape for various engineering structures, such as composites, adhesive pillars, and metamaterials[23-27] need only consider a few initial designs out of an infinitely large design space.

In this study, we utilize a machine learning based optimization approach to design the beam elements of lattice structures using Bézier curves, which is a concept originally used in the computer graphics field. Here, we adopt a BC lattice structure as our target to compare with previous work in the area of research. The shape of the beam elements is modeled by a high-order Bézier curve rather than a couple of critical radii to cover a more flexible design space. What is unique about Bézier curves is not just an opened up flexible design space but also it guarantees smooth surfaces in the domain. Smooth surfaces are especially important when it comes to manufacturing, ensuring that all the structures generated from our approach will be realizable for future practical applications. The relative density and modulus of the lattice structure are predicted through finite element analysis (FEA) and homogenization; initial data are obtained by using randomly generated Bézier curve control points. Then, two deep NNs are trained to predict the relative density and relative Young's modulus using the shape of the Bézier curve as an input. We then generate new beam element shapes by applying a hybrid NN and genetic optimization (GO) adaptive method for the creation of novel material structures. The optimized design is compared with two state-of-the-art models: (1) cylindrical beam that has one geometric parameter, radius, and (2) graded-density beam,[22] which is parameterized by two variables, the radii of the cross-section at the midpoint and ends of the beam element. The benefit of using a combined NN-GO approach compared to a simple GO method in accelerating the design approach is also discussed. Finally, we fabricate our optimized BC structure using additive manufacturing, and validate our optimized design with compression experiments.

Generative machine learning algorithm for shape optimization

The Bézier curve is adopted for modeling smooth beam elements in order to obtain lattice structures that can be accurately fabricated by additive manufacturing. A total of 20,000 different Bézier curves are obtained for initial datasets, and the elastic modulus and relative density of the BC truss are predicted using the method described in Fig. 1 and Computational methods section (ESI†). After preparing 20,000 initial datasets, we train two NNs considering the control points of the Bézier curve as input and the relative density or relative modulus as output. Fully connected networks including ten (relative density NN) and twelve (relative modulus NN) hidden layers are used, and the number of neurons in all hidden layers is the same as the input dimension. Batch normalization and ResNet architecture are employed to prevent gradient vanishing or boosting that may arise when training a deep neural network,[28] and leaky ReLu function with a linear slope of 0.1 is used as the activation function. The detailed architecture of the neural networks is depicted in Fig. S1 (ESI†). Here, details of the hyperparameters are discussed. The initial datasets are divided into a training and test set with a ratio of 9:1. The batch size is set to 1000 for the NN used to predict for relative density and 500 for the NN used to predict for relative modulus. The NNs are trained to minimize the root mean square

error (RMSE) by using the adaptive moment estimation (ADAM) optimizer[29] for 150 epochs. The initial learning rate is 0.01, and it is multiplied by 0.1 every 50 epochs. To verify the structures of our NN and the hyperparameters, the RMSE of the test set is calculated at every epoch.

Then, new Bézier curves are generated using GO and greedy decisions. The penalty function is employed to establish our objective function in order to find the optimized structure satisfying relative density constraints. The objective function (F) used in our study is

$$F(\bar{\rho},\bar{E}) = k|\bar{\rho} - \bar{\rho}_0| + \bar{E} \quad (5)$$

where $\bar{\rho}$ and $\bar{E}$ refer to relative density and modulus, respectively, and k represents the penalty coefficient. When the objective function is maximized using a negative penalty coefficient, the converged structure has maximized modulus with the relative density of $\bar{\rho}_0$. When the term $|\bar{\rho} - \bar{\rho}_0|$ is too small, the objective function does not have the maximum value at $\bar{\rho}_0$. In this study, we use -5 as the penalty coefficient so that the objective function has a maximum at $\bar{\rho}_0$ for the entire range of relative density (Fig. S2, ESI†). We also predict minimum Young's modulus of BC lattice structure by using a positive penalty coefficient. That is, the objective function is maximized when k=-5, or minimized when k=5, obtaining the optimized lattice structure with maximum or minimum Young's modulus, respectively. Using the relative density and modulus obtained from FEA, the outputs of all data are calculated through the objective function. In order to select the parent sets for applying to GO, the ranking is determined based on the output of the objective function; the top or bottom 5000 datasets are then selected as parent sets used for GO to maximize or minimize Young's modulus, respectively. For the GO, we consider the input data as a chromosome and each gene is the x or y coordinate of the control points, i.e., each chromosome contains 60 genes. After picking two different datasets from the parent sets, a new Bézier curve is obtained through a crossover product using a randomly selected division point, and random noise is applied to the parent set for mutation.

In our design approach, the objective function value of the offspring data is predicted from the two NNs, and it is accepted as a new dataset if the output is higher than the top 1% (when maximizing modulus) or lower than the bottom 1% (when minimizing modulus) of the total data. Since the NN provides fast predictions, we can make greedy decisions to select offspring with high outputs in terms of the objective function value. In order to prevent trapping into local minima during optimization, 500 random samples are generated at every generation and included in the new data set. When the number of newly created Bézier curves through GO reaches 1000, the ground truths of all new data are obtained through FEA and the homogenization method. Then, active learning is employed to increase the prediction accuracy of the NNs (Fig. 1d and Fig. S3, ESI†). The benefits of incorporating active learning in combination with NNs are to improve the prediction accuracy and decrease the extrapolation error. The NNs are updated by training with all datasets including new datasets generated by GO to expand the reliable prediction domain of NNs. After updating the NN, the top 5000 points are selected out of the total dataset (including all previous data) as parent sets and GO is then conducted. The optimized BC structures are obtained by this active learning-based optimization approach until convergence. We also conduct optimization using simple GO without NN-based acceleration to compare the design performance with our active learning-based optimization, and the same parameters are used for the calculation; a comparison of the methods is discussed in the next section along with the results.

Results & Discussion

During the training process of the two NNs, both the RMSEs of the training and test data sets decrease with increasing epoch and the RMSEs converge to a value lower than 10% of their initial values (Fig. 2). To verify the prediction accuracy of the trained NNs, we calculate R^2 by comparing the NN predictions against FEA results. The R^2 is calculated by fitting the data onto the y=x curve, and it represents the accuracy of the NN prediction. The R^2 of the test set of both the relative density and

modulus is higher than 99%, which implies high prediction accuracy (Fig. 2). We also calculate R^2 at every generation during optimization, and all of them are close to a value of 1 (Fig. S4, ESI†). Because of the high accuracy of the NN models, we are able to predict the properties without using expensive FEA calculations, which are roughly 50 times shower than the NNs. Moreover, FEA requires a large computational cost when the relative density is high because many elements are used for structures with more volume. However, since the prediction of the NNs is based on an algebraic calculation using control points as an input, the computation time does not depend on the relative density. Hence, if we employ the NNs as surrogate models when applying GO, we are able to quickly predict the output of the offspring data, which makes possible the use of greedy offspring selection.

In order to compare our optimized beam shape with the other models suggested by previous work,[22] the relative density of the BC lattice structure is fixed at the $\bar{\rho}_0 = 0.1734$ used in previous designs. As the generation of GO increases, the output of the objective function increases, and the datasets converge to the vertex of $\bar{\rho} = \bar{\rho}_0$ and $\bar{E} = \bar{E}_{\max}$. In particular, the minimum value of the last generation has a higher value than the maximum of the initial data (Fig. 3a). In other words, we are able to generate data having a higher value than the initial data by using active learning-based optimization. When optimization is performed by using simple GO, it has a lower modulus compared to our NN-GO design approach at every generation. For example, the maximum stiffness of the 8th simple GO generation is lower than that of the first generation of our design approach (Fig. 3b). Although active learning-based design requires computation time for training NNs, our method is much faster than simple GO due to the greedy decision. Moreover, simple GO requires more generations to obtain a comparable output, which results in increased computation time compared to our active learning-based design method. In particular, since the FEA analysis for one simulation takes a long time, the simple GO would take about ten times longer than our design method to obtain comparable output (Fig. S5, ESI†).

We compare the optimized design with two state-of-the-art models, the cylindrical beam (CL) and graded-density beam (GR).[22, 30-32] In order to investigate the effect of the beam shape on the mechanical properties of the lattice, the same material for all designs are used for simulation. The relative modulus of our optimized design is 0.0122, which is 21% and 77% higher than that of the GR and CL models, respectively. Our optimized shape has a larger radius variation compared to the GR model and is almost symmetrical at $x = \sqrt{3}a/4$ (Fig. 3c). One of the possible causes of the symmetric shape is the crystallographic symmetry of the BC structure. In fact, the $[111]$ and $[\bar{1}\bar{1}\bar{1}]$ of BC lattice are in the same family of directions, and the only way to satisfy the crystallographic symmetry for fully periodic lattice structure is having symmetric beam geometry. We also design an optimized shape using the symmetric 30th-order Bézier curve to validate our result, finding a negligible difference between the two cases (Fig. S6, ESI†).

The normalized effective stress fields of beam elements for the three structures are depicted in Fig. 3d and e. It can be noted that for any BC lattice structure there will a stress concentration near the joint region, the central part of the unit cell where the beam elements intersect, due to bending stress. For the CL model, the stress concentration near the joint area is higher than the GR and our model because it does not have much bending rigidity due to its uniform cross-sectional area. Similar to the CL model, the GR model also experiences high localized stress concentration at the joint region where it has a relatively small cross-sectional area. On the other hand, our model has a larger radius variation and more distributed stress field in comparison to the other models. The distribution of the material for our model is smartly shifted more towards the joint region, which is the weakest location of the lattice structure. The architecture of our model strikes to balance between two modes of deformation: axial and bending. Because it is able to balance between these two deformation modes, our model has higher mechanical properties and is more efficient for load bearing and energy absorption.

In order to validate our machine learning-based optimized design, the compressive Young's moduli of the three lattice structures are measured using additive manufacturing and experiments. Stereolithography (SLA) is used to fabricate the three BC lattice structures (Fig. 4a and b); (1) our optimized design (Our model), (2) graded-density beam lattice structure (GR model),[22] and (3) simple BC lattice structure consisting of the cylindrical beams (CL model). The Form 3 SLA printer developed by Formlabs is utilized and white standard resin is used for the fabrication. The lattice structures are additively fabricated by selectively curing the polymer resin layer-by-layer using an ultraviolet laser beam. The thickness of each layer is 50 μm and the liquid resin is solidified through the process. In order to fabricate accurate specimens, the lattice constant for the specimens is 1.5 cm which is much larger than the minimum feature size that can be fabricated by the 3D-printer, and a total of 27 unit cells (3×3×3) are used for the lattice structures. Using this fabrication method, we could fabricate the specimens without printing support structure inside the lattice structure except for the bottom side of the lattice. Since 3D-printing in general is a layer-by-layer additive approach to fabrication, the material waste is oftentimes reduced compared to a subtractive approach. The 3D-printing costs here depend mainly on the amount of material used for fabrication driven by the volume of the lattice structure. To this end, since the relative density of the three models is fixed, the same amount of resin is used. We conduct uniaxial compression testing using displacement control with a loading speed of 2 mm/min resulting in about 7.5×10^{-4} /s of strain rate. Three specimens are tested for each case (Our model, GR model, and CL model) to estimate the repeatability of our experiments, and the moduli are measured by using the slope of the linear portion of the curve within 1% ~ 2% of strain. Uniaxial compression testing is conducted to obtain the stiffness and strength of the lattice structures, and the stress-strain curves measured from our experiments are shown in Fig. 4c. The Young's moduli obtained from the experiments show good agreement with our simulation results as depicted in Fig. 4d. The GR model has higher stiffness than the CL model and our optimized design has modulus values 23% and 58% higher than that of the GR and CL models, respectively.

The strength of the lattice structures is measured using peak stress in the stress-strain curve obtained from experimental testing. It can be shown in Fig. 4e that the optimized design has 17% and 105% higher strength than the GR and CL models, respectively (Fig. 4e). The maximum normalized von Mises stress of our optimized design is lower than that of the other structures under the same applied loading, which is believed to be one of the reasons that our model has high strength properties. Because our designs are generated based on high order Bézier curves, the extra design flexibility allows for a smoother transition between the beam elements which reduces the overall stress concentration profile. In our experimental results, all of the fractures occur on the {111} plane where maximum shear stress is applied when the loading is applied in [100] direction for BC structure as shown in Fig. 4f. The fracture behavior of the lattice structures depends on the stress field within the beam elements. The two state-of-the-art models show one type of fracture at the joint because they have a highly concentrated stress field near the joint. On the other hand, in the optimized design, two types of fracture are observed because the stress near the joint is comparable to the stress at the smallest cross-section. Because the mechanism of increasing mechanical property is the same for both elastic modulus and strength, the optimized structure has the highest strength when optimizing elastic modulus under fixed lattice structure and density. Currently, our problem is trained on a linear elastic system with only the structure as input since any change in the material properties linearly scales the performance of any structure. It is of note that if instead we are working with a nonlinear system with large deformation or buckling occurring, optimized designs are expected to be different. These mechanisms can be taken into account if our ML model is modified to take as input not only structure but also base material properties, which would be an interesting future work.

To predict the lower bound of the relative Young's modulus of the BC structure, we minimize the objective function using $k = 5$ and $\bar{\rho} = 0.8$. The modulus decreases as the generation increases and it converges to a small relative modulus (Fig. 5a). One of the noticeable geometric changes in the lattice structure is that the cross-section area near the vertices of the unit cell gradually decreases, and

more stress is concentrated near the vertex as the optimization progresses (Fig. 5b). The cross-section of the final optimized structure is very small, and the modulus is very low due to the highly concentrated stress field. In fact, the minimum radius of the Bézier curve is set to $0.01a$ when creating the Bézier curve and thus the optimized structure has a finite section at the vertex. With no minimum radius constraint, the optimized design has an infinitesimally small cross-section at the vertex. Due to the small cross-section, the stress singularity rises at the vertices of the unit cell and the theoretical lower bound of modulus converges to zero because infinite stress is applied even under small loading. Hence, the theoretical lower bound of the relative modulus of the BC structure is zero regardless of the relative density.

We design the optimized beam shape of the BC structure for different relative densities to estimate the upper bound of the Young's modulus. Here a symmetric 30th-order Bézier curve is used for modeling the shape of the beam element and the same design approach is applied. The maximized Young's moduli are much higher than that of the typical BC structure composed of cylindrical beams for the entire range of relative density (0 – 1), as shown in Fig. 5c. The Gibson-Ashby power law, commonly used as an empirical model for describing the relationship between modulus and density of lattice structures, is employed to study the effects of relative density.[33-36] The power law is expressed as $\overline{E} = C\overline{\rho}^n$ where C and n are coefficients depending on the lattice types and our results are fitted to the expression under fixed C=1 to satisfy $\overline{E} = 1$ when $\overline{\rho} = 1$, i.e., only one fitting parameter n is used. From our simulation results, the maximum Young's modulus curve is obtained which is found to be accurate in the entire range of the relative density. The coordinates of all control points used for modeling the optimized Bézier curves are described in ESI†. The optimized curve for low relative density has a single undulation site at the middle of the curve and the optimized shapes at high density have more local minimum radii depicted in Fig. 5e. Since the stress is concentrated at the undulation sites, it results in a more distributed stress field and high stiffness. Interestingly, as the density increases, the topology of the structure is changed. When the density is high, the optimized structure contains a hole in the joint where the four beams intersect because lower stress is applied to the joint compared to the interface of the upper and lower beam elements (Fig. 5d). Hence, it is possible to obtain optimized structures allowing topology change by using our active learning-based design method. A generative design method combined with NNs has the advantage of being able to function without domain knowledge but requires a lot of training data to analyze the relationships accurately. In other words, if a small number of datasets are used for initial training, many iterations would be required during the active learning and optimization process. Therefore, in order to optimize, for example, nonlinear systems with large deformation with reasonable computational costs for future works, it is important to further understand the trade-off between the number of datasets and optimization performance.

Conclusions

In this study, the optimized beam shape of the BC lattice structure with maximum modulus and strength is designed using an active deep learning-based optimization approach. The optimized lattice structure and two other benchmark designs are fabricated by additive manufacturing and their mechanical properties are measured in experiments. We show that our optimized design has higher stiffness and strength than the benchmark ones and the fundamental mechanisms are explained by the distributed stress field predicted from our FEA. The lattice structures with the minimum modulus are also generated using the same method. Thus, the upper and lower bounds for the modulus over the entire range of relative density are proposed. Active deep learning-based optimization holds great promise in improving the mechanical properties of complex lattice structures such as octet, body-centered cubic, or face-centered cubic structures composed of two or more types of beam elements. To consider more types of beam shapes, the lattice structures need to be optimized with more input features. As an extension to this work, other mechanical properties essential for structural stability design such as fracture toughness, impact resistance, or buckling strength, can be optimized by training

NNs to learn the relationship between the input features and the desired properties.

Conflicts of interest

There are no conflicts of interest to declare.

Acknowledgements

This research was supported by Basic Science Research Program through the National Research Foundation of Korea (NRF) funded by the Ministry of Education (2020R1A6A3A03039104). The authors also acknowledge support from the Hellman Fellows Program and the Office of Naval Research (Fund Number: N00014-21-1-2604).

References

1. L. Choisez, L. Ding, M. Marteleur, H. Idrissi, T. Pardoen and P. J. Jacques, *Nat Commun*, 2020, **11**.
2. Y.-Y. Tsai, Y. Chiang, J. L. Buford, M.-L. Tsai, H.-C. Chen and S.-W. Chang, *ACS Biomaterials Science & Engineering*, 2021.
3. Y. Y. Chen, Z. Jia and L. F. Wang, *Compos Struct*, 2016, **152**, 395-402.
4. C.-T. Chen, D. C. Chrzan and G. X. Gu, *Nature communications*, 2020, **11**, 1-9.
5. M. K. Habibi, L.-h. Tam, D. Lau and Y. Lu, *Mechanics of Materials*, 2016, **97**, 184-198.
6. G. X. Gu, M. Takaffoli and M. J. Buehler, *Advanced Materials*, 2017, **29**, 1700060.
7. J. Bauer, A. Schroer, R. Schwaiger and O. Kraft, *Nat Mater*, 2016, **15**, 438-+.
8. C. M. Portela, B. W. Edwards, D. Veysset, Y. C. Sun, K. A. Nelson, D. M. Kochmann and J. R. Greer, *Nat Mater*, 2021.
9. J. K. Wilt, C. Yang and G. X. Gu, *Advanced Engineering Materials*, 2020, **22**, 1901266.
10. M. S. Pham, C. Liu, I. Todd and J. Lertthanasarn, *Nature*, 2019, **567**, E14-E14.
11. T. T. Li, Y. Y. Chen, X. Y. Hu, Y. B. Li and L. F. Wang, *Mater Design*, 2018, **142**, 247-258.
12. Z. Jin, Z. Zhang, K. Demir and G. X. Gu, *Matter*, 2020, **3**, 1541-1556.
13. N. Guo and M. C. Leu, *Frontiers of Mechanical Engineering*, 2013, **8**, 215-243.
14. Z. Jin, Z. Zhang, J. Ott and G. X. Gu, *Additive Manufacturing*, 2021, **37**, 101696.
15. Z. Vangelatos, G. X. Gu and C. P. Grigoropoulos, *Extreme Mechanics Letters*, 2019, **33**, 100580.
16. P. F. Egan, V. C. Gonella, M. Engensperger, S. J. Ferguson and K. Shea, *Plos One*, 2017, **12**.
17. W. Voigt, *Annalen der Physik*, 1889, **274**, 573-587.
18. L. R. Meza, A. J. Zelhofer, N. Clarke, A. J. Mateos, D. M. Kochmann and J. R. Greer, *P Natl Acad Sci USA*, 2015, **112**, 11502-11507.
19. L. Dong, *Acta Mater*, 2019, **175**, 90-106.
20. X. Zhang, A. Vyatskikh, H. J. Gao, J. R. Greer and X. Y. Li, *P Natl Acad Sci USA*, 2019, **116**, 6665-6672.
21. T. Tancogne-Dejean and D. Mohr, *Int J Mech Sci*, 2018, **141**, 101-116.
22. L. Bai, C. Y. Yi, X. H. Chen, Y. X. Sun and J. F. Zhang, *Materials*, 2019, **12**.
23. Y. Kim, C. Yang, Y. Kim, G. X. Gu and S. Ryu, *Acs Appl Mater Inter*, 2020, **12**, 24458-24465.
24. W. Ma, F. Cheng and Y. M. Liu, *Acs Nano*, 2018, **12**, 6326-6334.
25. C. T. Chen and G. X. Gu, *Adv Sci*, 2020, **7**.
26. L. L. Wu, L. Liu, Y. Wang, Z. R. Zhai, H. L. Zhuang, D. Krishnaraju, Q. X. Wang and H. Q. Jiang, *Extreme Mech Lett*, 2020, **36**.
27. D. Son, V. Liimatainen and M. Sitti, *Small*, 2021.
28. K. He, X. Zhang, S. Ren and J. Sun, 2016.
29. D. P. Kingma and J. Ba, *arXiv e-prints*, 2014, arXiv:1412.6980.
30. Y. B. Liu, Z. C. Dong, J. R. Ge, X. H. Lin and J. Liang, *Compos Struct*, 2019, **230**.
31. T. A. Alwattar and A. Mian, *Journal of Composites Science*, 2019, **3**.
32. L. Xiao, X. Xu, W. Song and M. Hu, *Materials*, 2020, **13**.

33. M. F. Ashby, *Metall Trans A*, 1983, **14**, 1755-1769.
34. L. R. Meza, S. Das and J. R. Greer, *Science*, 2014, **345**, 1322-1326.
35. N. Lavoine and L. Bergstrom, *J Mater Chem A*, 2017, **5**, 16105-16117.
36. Z. Z. Cai, Z. H. Liu, X. D. Hu, H. K. Kuang and J. S. Zhai, *Bio-Des Manuf*, 2019, **2**, 242-255.

Figures and captions

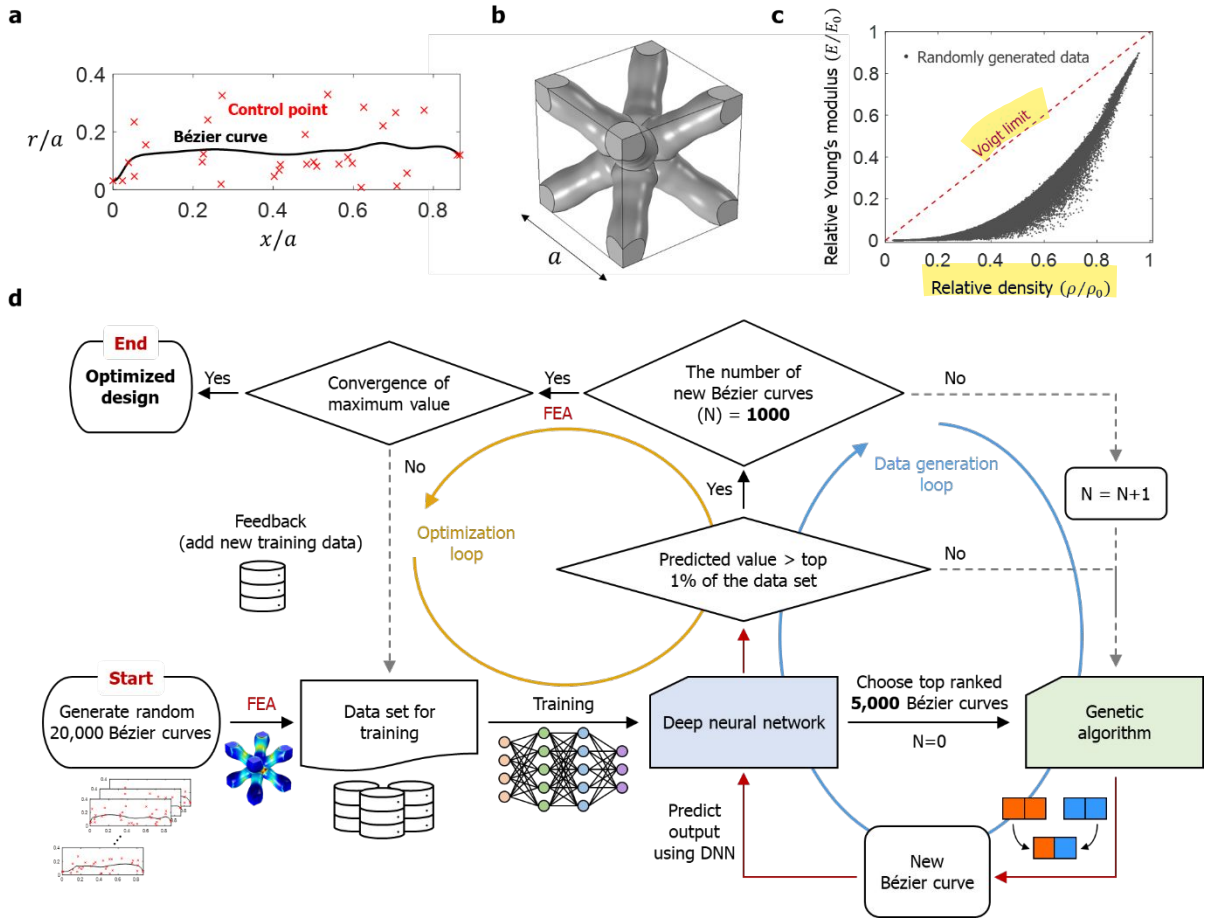

Fig. 1 (a) The 30th-order Bézier curve with control points where a is the lattice constant. The control points are described as red markers. (b) The unit cell of BC structure obtained using Bézier curve in (a). (c) The relative modulus – relative density plot of initial datasets. The initial datasets are obtained from randomly generated control points sets and the relative density has uniform distribution. (d) Workflow chart of our NN-GO design approach. The shape of the beam elements in the BC lattice structure is described by the Bézier curve with control points, and then the relative density and Young's modulus of the lattice structure are predicted from the FEA and homogenization method. Two different NNs are trained to predict the density and modulus using the control points as input. Then, applying to GO combined with the NNs, new beam shapes having high stiffness are derived as offspring. The NNs are updated by augmenting the new datasets generated by GO to improve the prediction accuracy, and the optimized beam shape is obtained by iterating the feedback process (active learning) between NN training and GO until convergence.

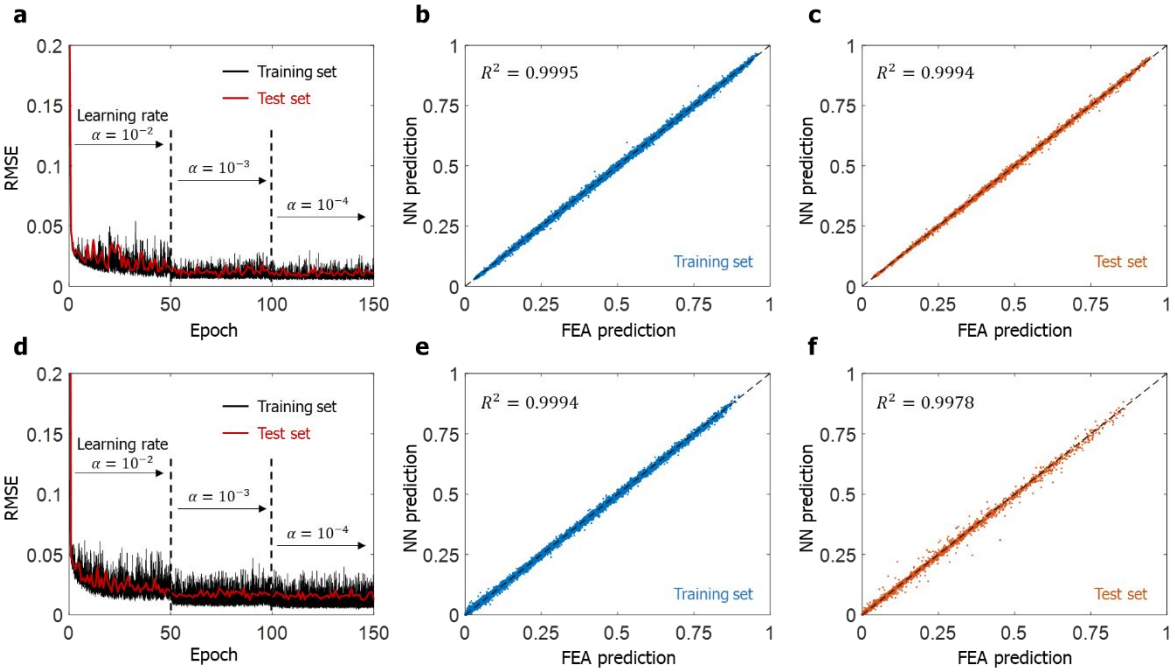

Fig. 2 The RMSE-epoch plot of NN that is used to predict (a) relative density and (d) relative modulus. Relative density of (b) training set and (c) test set predicted from NN with respect to FEA results. The relative Young's modulus of (e) training set and (f) test set predicted from NN compared to FEA results. The black dashed line in (b),(c),(e), and (f) is y=x.

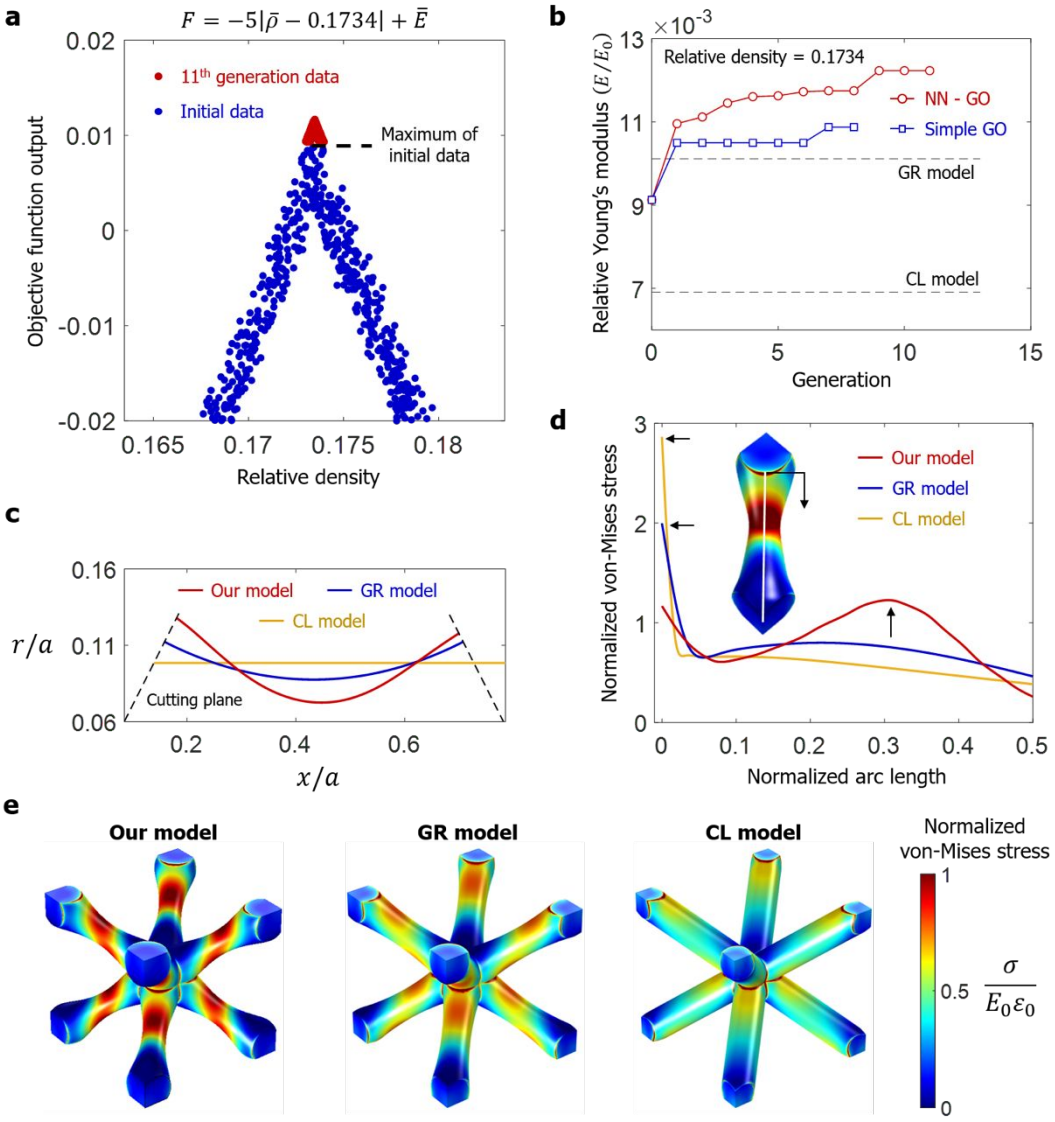

Fig. 3 (a) Scatter plot of objective function outputs at different generations as a function of relative density. (b) The relative Young's modulus as a function of the generation of GO for comparing NN-GO and base GO approaches. (c) Geometrical parameters for our model, GR model, and CL model; lengths are normalized by the lattice constant, a. (d) Normalized von Mises stress along the line on the beam surface and the arc length is the distance from the joint. The arrows indicate maximum stress of each beam element. (e) Stress plot within unit cells of the three BC structures. The E_0 is the Young's modulus of base material and ε_0 is the applied uniaxial strain.

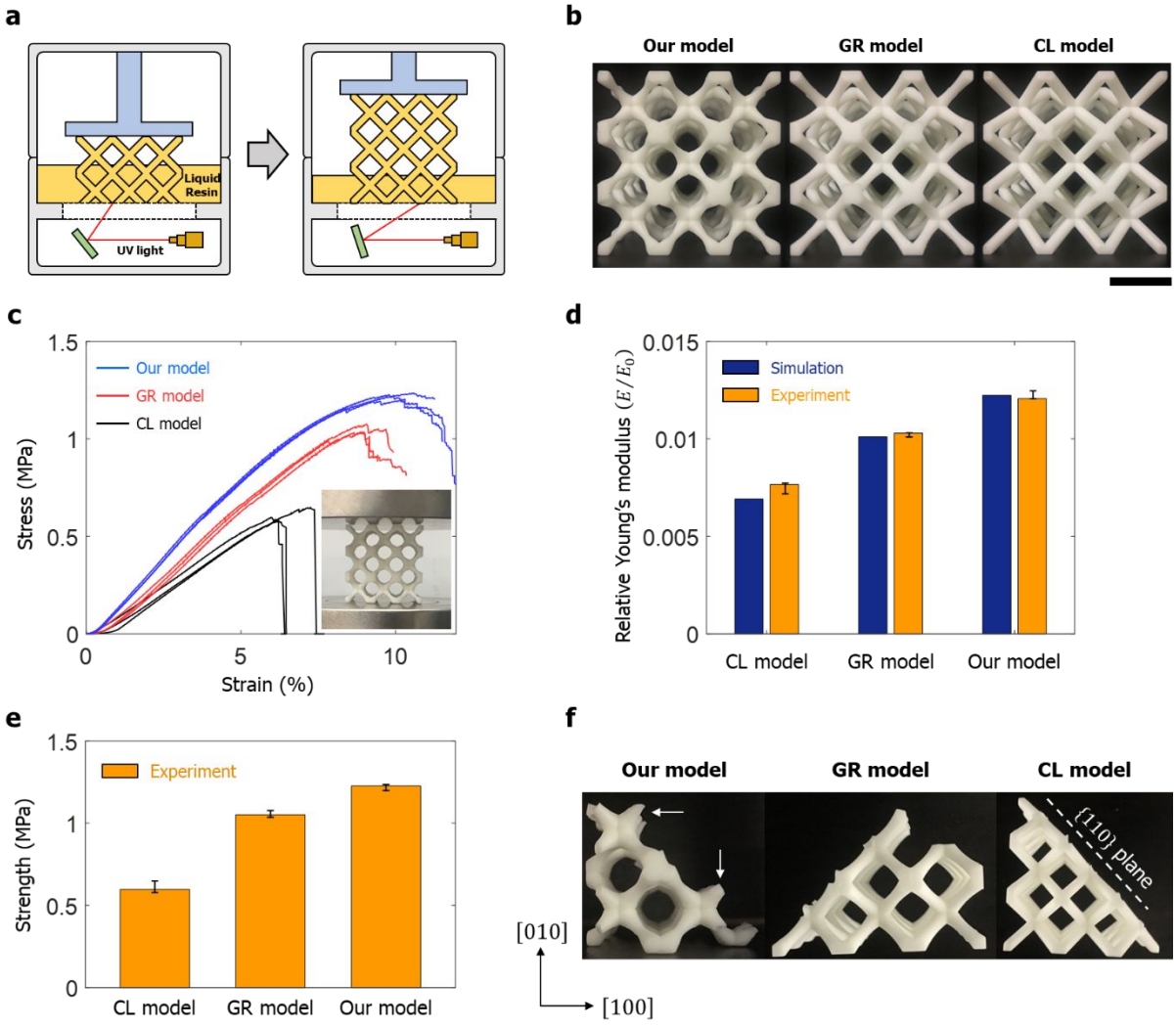

Fig. 4 (a) Schematic of SLA 3D-printing process. (b) Three different specimens (Our model, GR model, and CL model) printed by SLA. The black line at the right bottom represents a scale bar of 1.5 cm. (c) Stress-strain curves of the three lattice structures. (d) Relative Young's moduli and e) strength of the three BC structures. (f) Three lattice structures after fracture. One fracture type is observed at the joint in GR and CL model, and Our model shows an additional type which occurs at the small cross-section of beam element (white arrows in the figure).

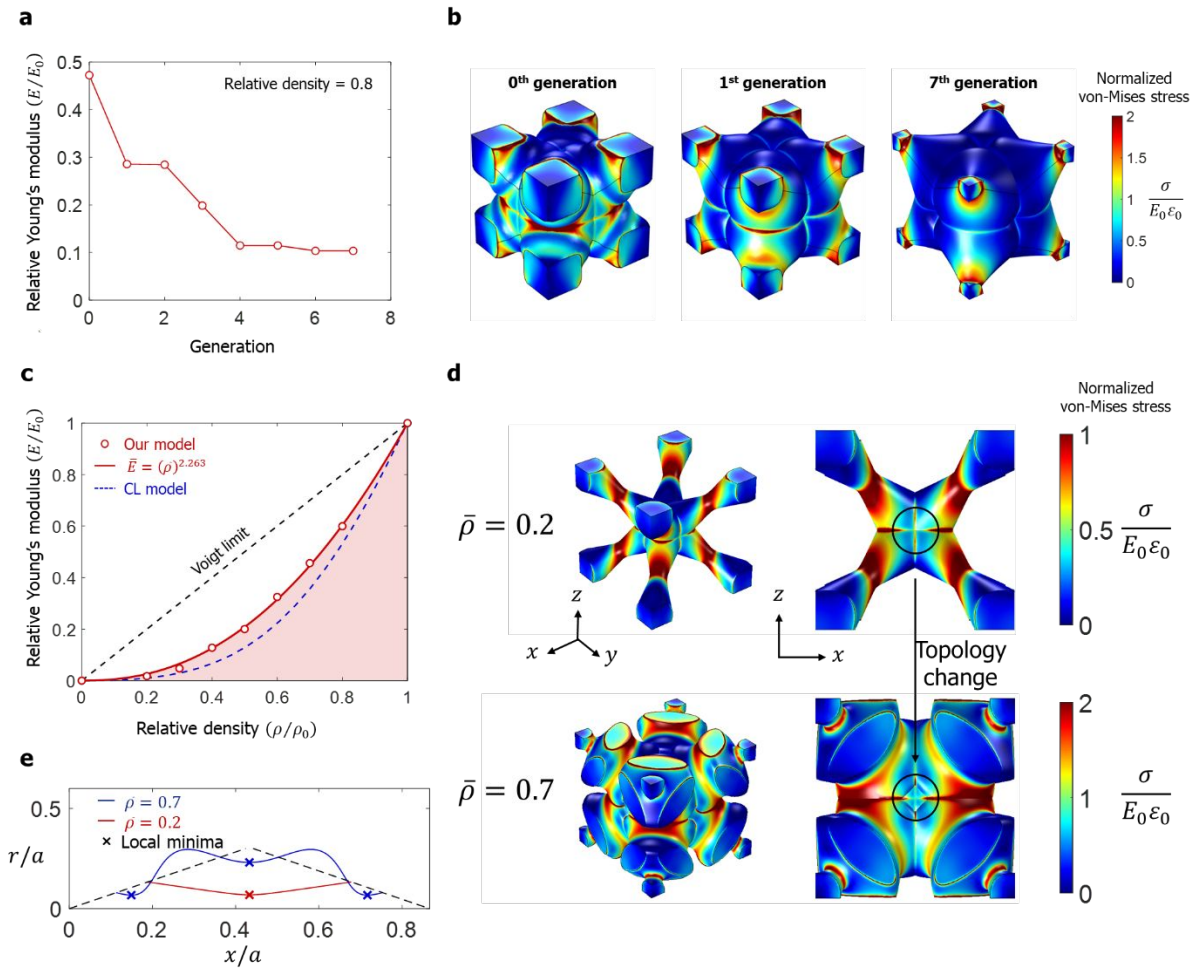

Fig. 5 Optimization results for minimizing stiffness of lattice structure with relative density of 0.8. (a) Relative Young's modulus with respect to generation of GO. (b) The von Mises stress plot at different generations. As optimization progresses, the area of sliced surface at the vertices of unit cell decreases resulting in high stress concentration. (c) Maximum relative Young's modulus of the lattice structure for relative density. As the theoretical lower bound is zero for the entire range of relative density, the red shaded area represents the relative modulus that BC lattice structures can have. (d) The von Mises stress of BC structure at two different relative densities. (e) Bézier curves for optimized beam elements. The curve has one local minimum at $\bar{\rho} = 0.2$ and there are three local minima at $\bar{\rho} = 0.7$.